Nanoscale Research Letters
a SpringerOpen Journal

NANO EXPRESS Open Access

Photocatalytic reduction synthesis of $SrTiO_3$-graphene nanocomposites and their enhanced photocatalytic activity

Tao Xian[1,2], Hua Yang[1,2*], Lijing Di[2], Jinyuan Ma[1], Haimin Zhang[2] and Jianfeng Dai[1,2]

Abstract

$SrTiO_3$-graphene nanocomposites were prepared via photocatalytic reduction of graphene oxide by UV light-irradiated $SrTiO_3$ nanoparticles. Fourier transformed infrared spectroscopy analysis indicates that graphene oxide is reduced into graphene. Transmission electron microscope observation shows that $SrTiO_3$ nanoparticles are well assembled onto graphene sheets. The photocatalytic activity of as-prepared $SrTiO_3$-graphene composites was evaluated by the degradation of acid orange 7 (AO7) under a 254-nm UV irradiation, revealing that the composites exhibit significantly enhanced photocatalytic activity compared to the bare $SrTiO_3$ nanoparticles. This can be explained by the fact that photogenerated electrons are captured by graphene, leading to an increased separation and availability of electrons and holes for the photocatalytic reaction. Hydroxyl (·OH) radicals were detected by the photoluminescence technique using terephthalic acid as a probe molecule and were found to be produced over the irradiated $SrTiO_3$ nanoparticles and $SrTiO_3$-graphene composites; especially, an enhanced yield is observed for the latter. The influence of ethanol, KI, and N_2 on the photocatalytic efficiency was also investigated. Based on the experimental results, ·OH, h^+, and H_2O_2 are suggested to be the main active species in the photocatalytic degradation of AO7 by $SrTiO_3$-graphene composites.

Keywords: $SrTiO_3$-graphene nanocomposites; Photocatalysis; Photocatalytic mechanism
PACS: 61.46. + w; 78.67.Bf; 78.66.Sq

Background

Semiconductor photocatalysts have attracted considerable attention over the past decades due to their potential applications in solar energy conversion and environmental purification [1,2]. Among them, $SrTiO_3$, a well-known cubic perovskite-type multimetallic oxide with a bandgap energy (E_g) of approximately 3.2 eV, is proved to be a promising photocatalyst for water splitting and degradation of organic pollutants [3-6]. Furthermore, the photocatalytic activity of $SrTiO_3$ can be tailored or enhanced by doping with metalloid elements, decoration with noble metals, and composite with other semiconductors [7-10]. It is generally accepted that the basic principle of semiconductor photocatalysis involves the photogeneration of electron–hole (e^--h^+) pairs, migration of the photogenerated carriers to the photocatalyst surface, redox reaction of the carriers with other chemical species to produce active species (such as ·OH, $\cdot O_2$, and H_2O_2), and attack of the active species on pollutants leading to their degradation. In these processes, the high recombination rate of the photogenerated carries greatly limits the photocatalytic activity of catalysts. Therefore, the effective separation of photogenerated electron–hole pairs is very important in improving the photocatalytic efficiency.

Graphene, being a two-dimensional (2D) sheet of sp^2-hybridized carbon atoms, possesses unique properties including high electrical conductivity, electron mobility, thermal conductivity, mechanical strength, and chemical stability [11-13]. On account of its outstanding properties, graphene has been frequently used as an ideal support to integrate with a large number of functional nanomaterials to form nanocomposites with improved performances in the fields of photocatalysts [14-21], supercapacitors [22],

* Correspondence: hyang@lut.cn
[1]State Key Laboratory of Advanced Processing and Recycling of Non-ferrous Metals, Lanzhou University of Technology, Lanzhou 730050, People's Republic of China
[2]School of Science, Lanzhou University of Technology, Lanzhou 730050, People's Republic of China

field-emission emitters [23], and fuel cells [24]. Particularly, the combination of graphene with photocatalysts is demonstrated to be an efficient way to promote the separation of photogenerated electron–hole pairs and then enhance their photocatalytic activity [14-21]. In these photocatalyst-graphene composites, photogenerated electrons can be readily captured by graphene which acts as an electron acceptor, leading to an increasing availability of photogenerated electrons and holes participating in the photocatalytic reactions. But so far, the investigation concerning the photocatalytic performance of $SrTiO_3$-graphene nanocomposites has been rarely reported.

Up to now, semiconductor-graphene nanocomposites have been generally prepared using graphene oxide as the precursor, followed by its reduction to graphene. To reduce the graphene oxide, several methods have been employed including chemical reduction using hydrazine or $NaBH_4$ [14], high-temperature annealing reduction [15], hydrothermal reduction using supercritical water [16], green chemistry method [17], and photocatalytic reduction using semiconductors [18-21]. Among them, the photocatalytic reduction is an environment-friendly and a mild way for the synthesis of semiconductor-graphene composites. In this route, the solution containing the photocatalyst and graphene oxide is irradiated with light energy greater than the E_g of the photocatalyst, during which graphene oxide receives electrons from the excited photocatalyst and is thus reduced to graphene. During the photocatalytic reduction process, photocatalyst nanoparticles are assembled onto graphene sheets to form photocatalyst-graphene composites. Herein, we report the synthesis of $SrTiO_3$-graphene nanocomposites via the photocatalytic reduction method. The photocatalytic activity of the composites was evaluated by the degradation of acid orange 7 (AO7) under ultraviolet (UV) light irradiation, and the photocatalytic mechanism involved was discussed.

Methods

$SrTiO_3$ nanoparticles were synthesized via a polyacrylamide gel route as described in the literature [25]. The graphene oxide used in this research was purchased from Nan-Jing XF Nano Materials Tech Co. Ltd. (Nanjing, China). $SrTiO_3$-graphene composites were prepared via a photocatalytic reduction route. A certain amount of graphene oxide was dispersed in 50 mL distilled water, followed by ultrasonic treatment of the suspension for 30 min. Then, 0.1 g $SrTiO_3$ nanoparticles and 0.0125 g ammonium oxalate (AO) were added to the suspension under magnetic stirring. After stirring for 10 min, the mixture was purged with nitrogen and exposed to UV light irradiation from a 15-W low-pressure mercury lamp for 5 h under mild stirring. During the irradiation, the color of the mixture changed from brown to black, indicating the reduction of the graphene oxide. After that, the product was separated from the reaction solution by centrifugation at 4,000 rpm for 10 min, washed several times with distilled water and absolute ethanol, and then dried in a thermostat drying oven at 60°C for 4 h to obtain $SrTiO_3$-graphene composites. A series of samples were prepared by varying the weight fraction of graphene oxide from 2.5% to 10%.

The photocatalytic activity of the samples was evaluated by the degradation of AO7 under UV light irradiation of a 15-W low-pressure mercury lamp ($\lambda = 254$ nm). The initial AO7 concentration was 5 mg L^{-1} with a photocatalyst loading of 0.5 g L^{-1}. Prior to irradiation, the mixed solution was ultrasonically treated in the dark to make the photocatalyst uniformly dispersed. The concentration of AO7 after the photocatalytic degradation was determined by measuring the absorbance of the solution at a fixed wavelength of 484 nm. Before the absorbance measurements, the reaction solution was centrifuged for 10 min at 4,000 rpm to remove the photocatalyst. The degradation percentage is defined as $(C_0 - C_t) / C_0 \times 100\%$, where C_0 and C_t are the AO7 concentrations before and after irradiation, respectively. To investigate the photocatalytic stability of the $SrTiO_3$-graphene composites, the recycling tests for the degradation of AO7 using the composite were carried out. After the first cycle, the photocatalyst was collected by centrifugation, washed with water, and dried. The recovered photocatalyst was introduced to the fresh AO7 solution for the next cycle of the photocatalysis experiment under the same conditions. The process was repeated four times.

Terephthalic acid (TA) was used as a probe molecule to examine hydroxyl (·OH) radicals produced over the irradiated $SrTiO_3$-graphene composites. It is expected that TA reacts with $\cdot OH$ to generate a highly fluorescent compound, 2-hydroxyterephthalic acid (TAOH). By measuring the photoluminescence (PL) intensity of TAOH that is pronounced around 429 nm, the information about $\cdot OH$ can be obtained. TA was dissolved in a NaOH solution (1.0 mmol L^{-1}) to make a 0.25-mmol L^{-1} TA solution and then to the solution was added 0.5 g L^{-1} $SrTiO_3$-graphene composites. The mixed solution, after several minutes of ultrasound treatment in the dark, was illuminated under a 15-W low-pressure mercury lamp. The reacted solution was centrifuged for 10 min at 4,000 rpm to remove the photocatalyst and was then used for the PL measurements through a fluorescence spectrophotometer with the excitation wavelength of 315 nm.

The phase purity of the samples was examined by means of X-ray powder diffraction (XRD) with Cu Kα radiation. Fourier transform infrared spectroscopy (FTIR) measurements were carried out on a Bruker IFS 66v/S spectrometer (Ettlingen, Germany). The morphology of the samples was observed by a field emission transmission electron microscope (TEM). The UV-visible diffuse reflectance spectra

were measured using a UV-visible spectrophotometer with an integrating sphere attachment.

Results and discussion

Figure 1 schematically shows the photocatalytic reduction process of graphene oxide by UV light-irradiated $SrTiO_3$ nanoparticles. It is noted that the $SrTiO_3$ particles have an isoelectric point at pH 8.5 [26]; that is, they bear a negative surface charge when pH > 8.5 and a positive surface charge when pH < 8.5. When the $SrTiO_3$ particles are added to the graphene oxide suspension, the pH value of the mixture is measured to be approximately 6.5, implying that the $SrTiO_3$ particle surface is positively charged. On the other hand, the oxygen-containing functional groups of graphene oxide (such as carboxylic acid -COOH and hydroxyl -OH) are deprotonated when it immersed in water, which leads to negative charges created on graphene oxide [27]. As a result, the $SrTiO_3$ particles are expected to be adsorbed onto the graphene oxide sheets through electrostatic interactions. Upon UV-light irradiation, electrons and holes are produced on the conduction band (CB) and valence band (VB) of the $SrTiO_3$ particles, respectively. The photogenerated holes are captured by ammonium oxalate that is a hole scavenger [28], leaving behind the photogenerated electrons on the surface of the $SrTiO_3$ particles. The electrons are injected from the $SrTiO_3$ particles into the graphene oxide and react with its oxygen-containing functional groups to reduce graphene oxide.

Figure 2 shows the FTIR spectra of graphene oxide, $SrTiO_3$ particles, and $SrTiO_3$-graphene(10%) composites. In the spectrum of graphene oxide, the absorption peak at 1,726 cm^{-1} is caused by the C = O stretching vibration of the COOH group. The peak at 1,620 cm^{-1} is attributed to the C = C skeletal vibration of the graphene sheets. The absorption peak of O-H deformation vibrations in C-OH can be seen at 1,396 cm^{-1}. The absorption bands at around 1,224 and 1,050 cm^{-1} are assigned to the C-O stretching vibration. For the $SrTiO_3$ particles, the broad absorption bands at around 447 and 625 cm^{-1} correspond to TiO_6 octahedron bending and stretching vibration, respectively [29]. The absorption peak at around 1,630 cm^{-1} is due to the bending vibration of H-O-H from the adsorbed H_2O. In the spectrum of the $SrTiO_3$-graphene composites, the characteristic peaks of $SrTiO_3$ are detected. The absorption

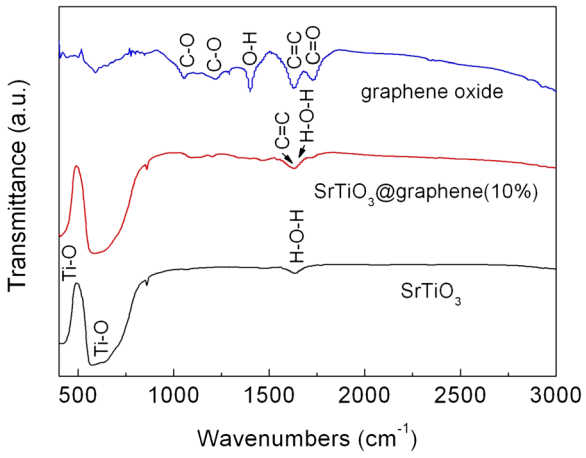

Figure 2 FTIR spectra of graphene oxide, $SrTiO_3$ particles, and $SrTiO_3$-graphene(10%) composites.

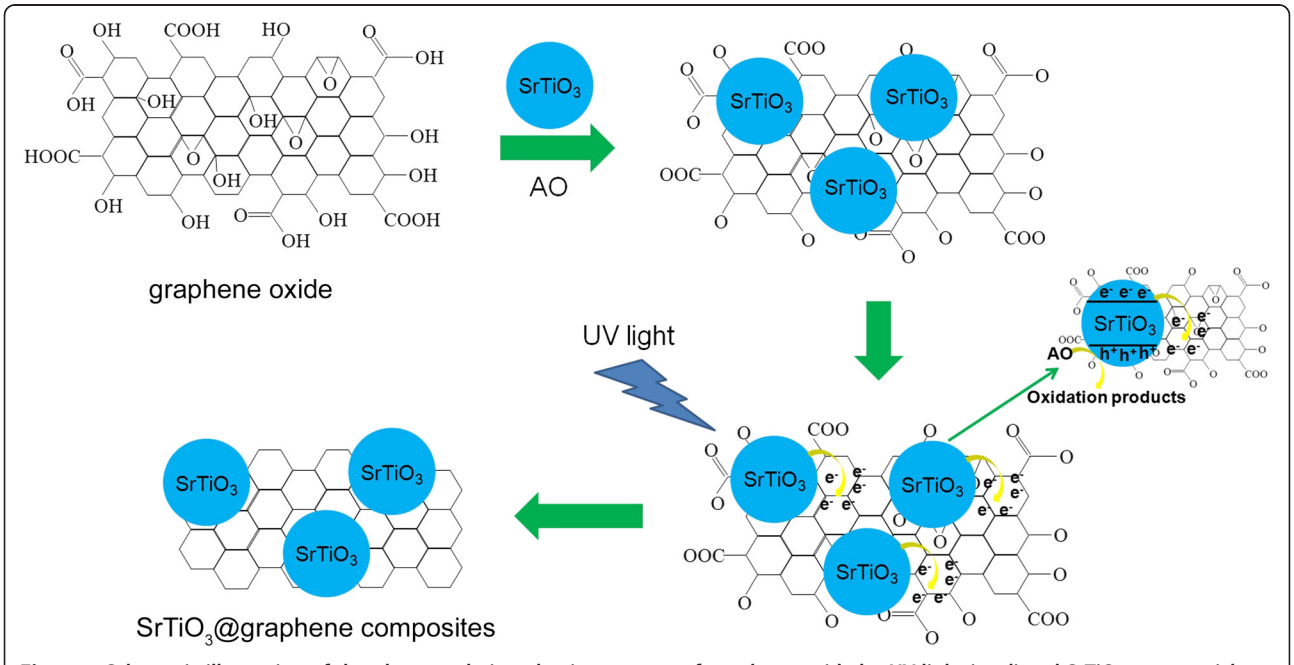

Figure 1 Schematic illustration of the photocatalytic reduction process of graphene oxide by UV light-irradiated $SrTiO_3$ nanoparticles.

peak at 1,630 cm^{-1} is the overlay of the vibration peak of H-O-H from H_2O and C = C skeletal vibration peak in the graphene sheets. However, the absorption peaks of oxygen-containing functional groups, being characteristic for graphene oxide, disappear. The results demonstrate that graphene oxide is completely reduced to graphene during the photocatalytic reduction process.

Figure 3 shows the XRD patterns of the $SrTiO_3$ particles and the $SrTiO_3$-graphene (10%) composites. It is seen that all the diffraction peaks for the bare $SrTiO_3$ particles and the composites can be index to the cubic structure of $SrTiO_3$, and no traces of impurity phases are detected. This indicates that the $SrTiO_3$ particles undergo no structural change after the photocatalytic reduction of graphene oxide. In addition, no apparent diffraction peaks of graphene in the composites are observed, which is due to the low content and relatively weak diffraction intensity of the graphene.

Figure 4a shows the TEM image of graphene oxide, indicating that it has a typical two-dimensional sheet structure with crumpled feature. Figure 4b shows the TEM image of the $SrTiO_3$ particles, revealing that the particles are nearly spherical in shape with an average size of about 55 nm. The TEM image of the $SrTiO_3$-graphene (10%) composites is presented in Figure 4c, from which one can see that the $SrTiO_3$ particles are well assembled onto the graphene sheet.

Figure 5a shows the UV-visible diffuse reflectance spectra of the $SrTiO_3$ particles and $SrTiO_3$-graphene composites. The composites display continuously enhanced light absorbance over the whole wavelength range with increasing graphene content. This can be attributed to the strong light absorption of graphene in the UV-visible light region [30]. Figure 5b shows the corresponding first derivative of the reflectance (R) with respect to wavelength λ (i.e., $dR / d\lambda$), where the peak wavelength is characterized to be the

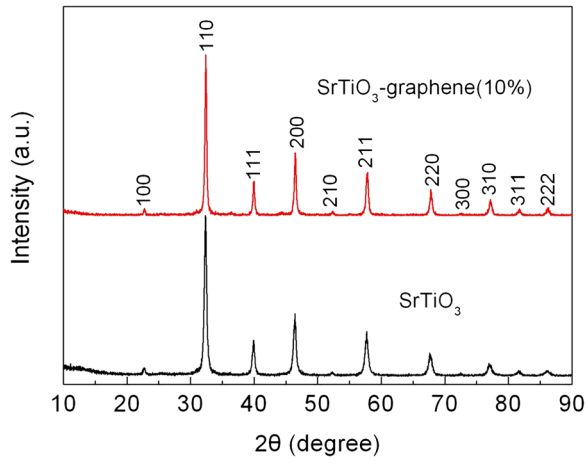

Figure 3 XRD patterns of the $SrTiO_3$ particles and $SrTiO_3$-graphene(10%) composites.

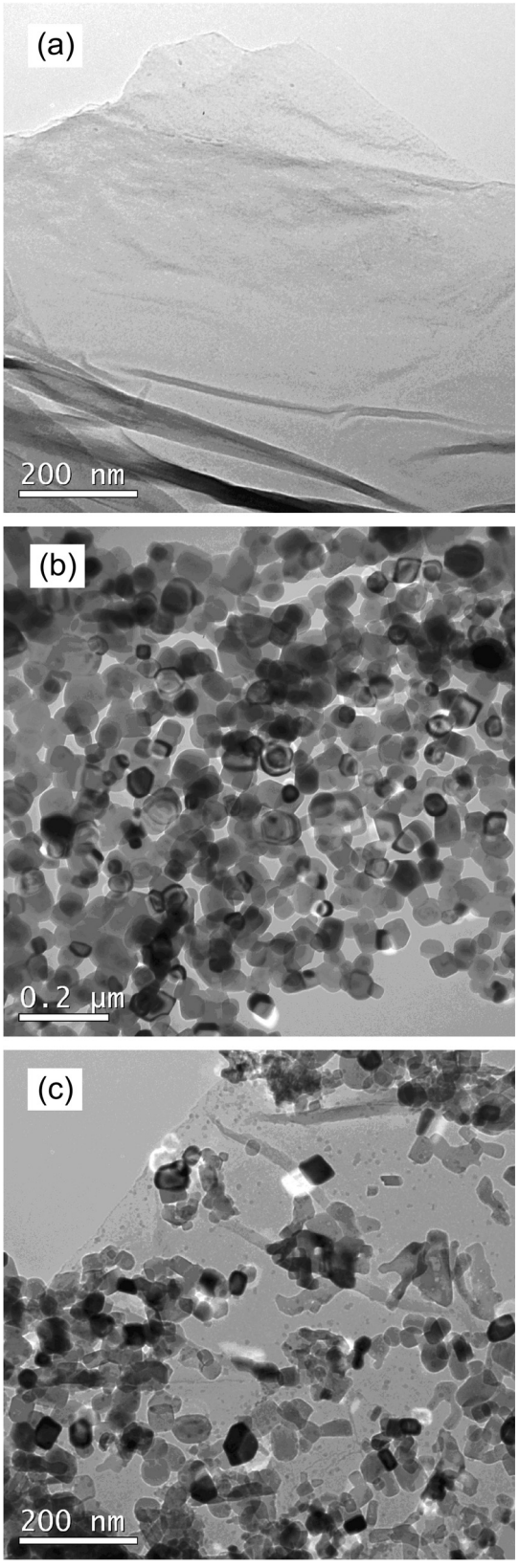

Figure 4 TEM images of (a) graphene oxide, (b) $SrTiO_3$ particles, and (c) $SrTiO_3$-graphene(10%) composites.

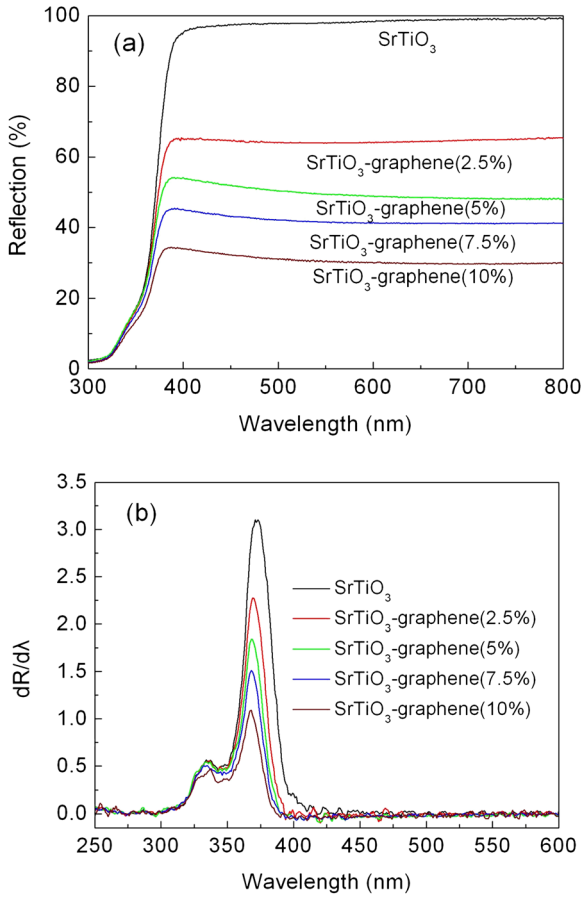

Figure 5 Diffuse reflectance spectra and corresponding first derivative. (a) Diffuse reflectance spectra of the samples. **(b)** Corresponding first derivative of diffuse reflectance spectra.

absorption edge of the samples. It is seen that the $SrTiO_3$ particles and composites present two absorption peaks in the derivative spectra. The strong and sharp absorption edge at approximately 370 nm is suggested to be attributed to the electron transition from valence band to conduction band. In comparison to the $SrTiO_3$ particles, the $SrTiO_3$-graphene composites show almost no shift in this absorption edge, indicating that the effect of graphene on the band structure of $SrTiO_3$ can be neglected. From this absorption edge, the E_g of the samples is obtained to be approximately 3.35 eV. In addition, the relatively weak absorption edge at approximately 335 nm may be ascribed to the surface effects.

The photocatalytic activity of the $SrTiO_3$-graphene composites was evaluated by the degradation of AO7 under UV light irradiation. Figure 6 shows the photocatalytic degradation of AO7 over the $SrTiO_3$-graphene composites as a function of irradiation time (t). The blank experiment result is also shown in Figure 6, from which one can see that AO7 is hardly degraded under UV light irradiation without photocatalysts, and its degradation percentage is less than

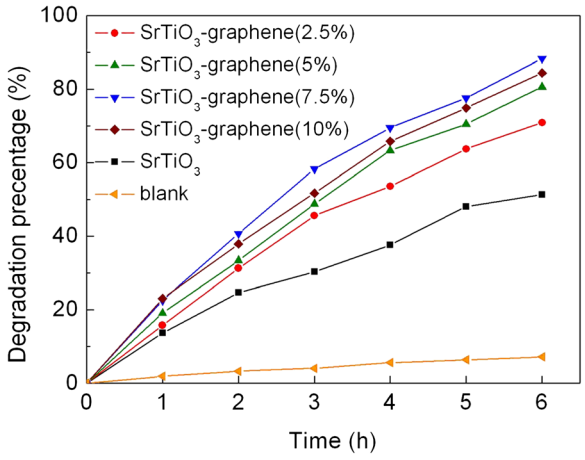

Figure 6 Photocatalytic degradation of AO7 over $SrTiO_3$ particles and $SrTiO_3$-graphene composites. This degradation is a function of irradiation time, along with the blank experiment result.

8% after 6 h of exposure. After the 6-h irradiation in the presence of $SrTiO_3$ particles, about 51% of AO7 is observed to be degraded. When the $SrTiO_3$ particles assembled on the graphene sheets, the obtained samples exhibit higher photocatalytic activity than the bare $SrTiO_3$ particles. In these composites, the photocatalytic activity increases gradually with increasing graphene content and achieves the highest value when the content of graphene reaches 7.5%, where the degradation of AO7 is about 88% after irradiation for 6 h. Further increase in graphene content leads to the decrease of the photocatalytic activity.

Figure 7 shows the PL spectra of the TA solution after reacting for 6 h over the UV light-irradiated $SrTiO_3$ particles and $SrTiO_3$-graphene(7.5%) composites. The blank experiment result indicates almost no PL signal at 429 nm after irradiation without photocatalyst. On irradiation in the presence of the $SrTiO_3$ particles, the PL signal

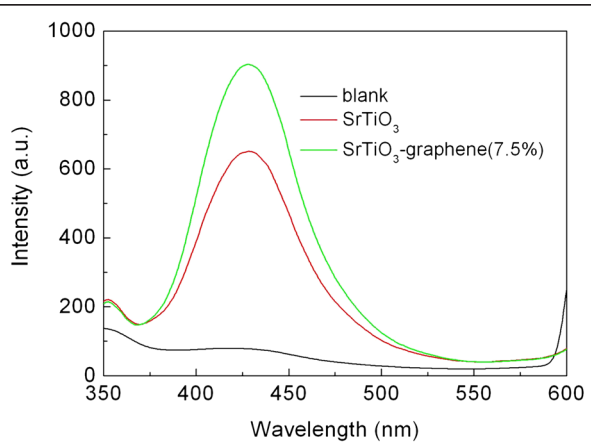

Figure 7 PL spectra of the TA solution after reacting for 6 h over the irradiated samples. The blank experiment result is also shown.

centered around 429 nm is obviously detected, revealing the generation of $\cdot OH$ radicals. When the $SrTiO_3$-graphene composites are used as the photocatalyst, the PL signal becomes more intense, suggesting that the yield of the $\cdot OH$ radicals is enhanced over the irradiated composites.

Generally, h^+, $\cdot OH$, $\cdot O_2$, and H_2O_2 are thought to be the main active species responsible for the dye degradation [31]. It is known that ethanol is a scavenger for $\cdot OH$, and KI is a scavenger for both $\cdot OH$ and h^+ [32,33]. By investigating the effect of ethanol and KI on the photocatalytic efficiency of the composites toward the AO7 degradation, we can clarify the role of h^+ and $\cdot OH$ in the photocatalysis. The role of $\cdot O_2$ and H_2O_2, which are derived from the reaction between dissolved O_2 and photogenerated e^-, on the dye degradation can be examined by investigating the effect of N_2 on the photocatalytic efficiency since the dissolved O_2 can be removed from the solution by the N_2-purging procedure. Figure 8 shows the effect of N_2 (bubbled at a rate of 0.1 L min^{-1}), ethanol (10% by volume), and KI (2×10^{-3} mol L^{-1}) on the degradation percentage of AO7 after 6 h of photocatalysis. It is demonstrated that when adding ethanol to the reaction solution, the photocatalytic degradation of AO7 undergoes a substantial decrease, from approximately 88% under normal condition to approximately 40% on addition of ethanol. This suggests that $\cdot OH$ radical is an important active species responsible for the dye degradation. Figure 7 provides direct evidence showing the generation of $\cdot OH$ radicals over the irradiated $SrTiO_3$-graphene composites. The addition of KI to the reaction solution results in a higher suppression of the photocatalytic efficiency compared to the addition of ethanol, where only 16% of AO7 is caused to be degraded, indicating that the photogenerated h^+ also plays a role in the degradation of AO7. In addition, the photocatalytic efficiency decreases slightly under N_2-purging condition, implying comparatively minor role of $\cdot O_2$ and/or H_2O_2 for the dye degradation.

In order to understand the photocatalytic mechanism of semiconductor-based photocatalysts, it is essential to determine their energy-band potentials since the redox ability of photogenerated carriers is associated with energy-band potentials of photocatalysts. The conduction band and valence band potentials of $SrTiO_3$ can be calculated using the following relation [34]:

$$E_{CB} = X - E^e - 0.5E_g$$
$$E_{VB} = E_{CB} + E_g, \quad (1)$$

where X is the absolute electronegativity of $SrTiO_3$ (defined as the arithmetic mean of the electron affinity and the first ionization of the constituent atoms) and estimated to be 5.34 eV according to the data reported in the literature [35,36], E^e is the energy of free electrons on the hydrogen scale (4.5 eV), and E_g is the bandgap energy of $SrTiO_3$ (3.35 eV). The conduction band and valence band potentials of $SrTiO_3$ vs. normal hydrogen electrode (NHE) are therefore calculated to be $E_{CB} = -0.84$ V and $E_{VB} = +2.51$ V, respectively.

Based on the obtained experimental results, a possible photocatalytic mechanism of $SrTiO_3$-graphene composites toward the degradation of AO7 is schematically shown in Figure 9. When $SrTiO_3$ is irradiated with light of energy greater than its bandgap energy, electrons are excited to the conduction band from the valence band, thus creating electron–hole pairs (Equation 2). Generally, most of the photogenerated electrons and holes recombine rapidly, and only a few of them participate in redox reactions. It is noted that graphene, which is an excellent electron acceptor and conductor, has a Fermi level (−0.08 V vs. NHE [37]) positive to the conduction band potential of $SrTiO_3$ (−0.84 V). When $SrTiO_3$ particles

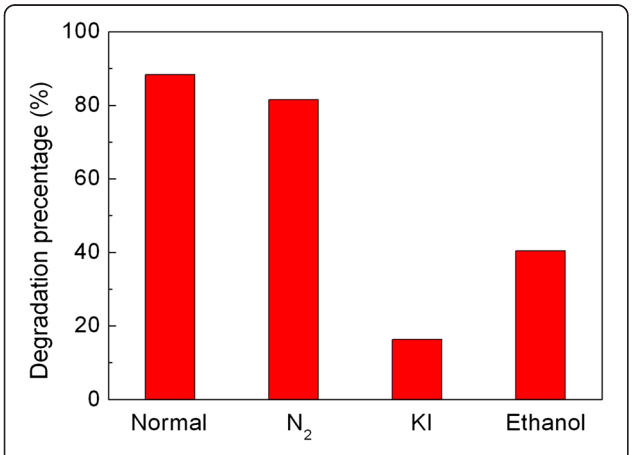

Figure 8 Effects of N_2, ethanol, and KI on the degradation percentage of AO7 over $SrTiO_3$-graphene(7.5%) composites. The irradiation time is 6 h.

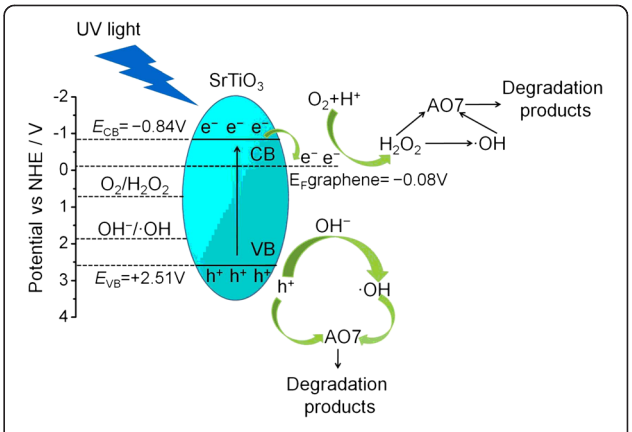

Figure 9 Schematic illustration of the photocatalytic mechanism of $SrTiO_3$-graphene composites toward the degradation of AO7.

are assembled onto graphene sheets, the photogenerated electrons can readily transfer from the conduction band of $SrTiO_3$ to graphene (Equation 3). Thus, the recombination of electron–hole pairs can be effectively suppressed in the composites, which leads to an increased availability of electrons and holes for the photocatalytic reactions. The Fermi level of graphene is positive to the redox potential of $O_2/\cdot O_2$ (−0.13 V vs. NHE) but negative to that of O_2/H_2O_2 (+0.695 vs. NHE) [31,38]. This implies that the photogenerated e^- which transferred onto the graphene cannot thermodynamically react with O_2 to produce $\cdot O_2$, but can react with O_2 and H^+ to produce H_2O_2 (Equation 4). H_2O_2 is an active species that can cause dye degradation, and moreover, H_2O_2 can also participate in the reactions as described in Equations 5 and 6 to form another active species $\cdot OH$. The valence band potential of $SrTiO_3$ (+2.51 V) is positive to the redox potential of $OH^-/\cdot OH$ (+1.89 V vs. NHE) [39], indicating that the photogenerated h^+ can react with OH^- to produce $\cdot OH$ (Equation 7). As a consequence, the active species $\cdot OH$, h^+, and H_2O_2 work together to degrade AO7 (Equation 8).

$$SrTiO_3 + h\nu \rightarrow SrTiO_3\left(e^- + h^+\right) \quad (2)$$

$$e^- + \text{Graphene} \rightarrow \text{Graphene}\left(e^-\right) \quad (3)$$

$$2\,\text{Graphene}\left(e^-\right) + O_2 + 2H^+ \rightarrow 2\,\text{Graphene} + H_2O_2 \quad (4)$$

$$H_2O_2 + h\nu \rightarrow 2\cdot OH \quad (5)$$

$$H_2O_2 + e^- \rightarrow \cdot OH + OH^- \quad (6)$$

$$h^+ + OH^- \rightarrow \cdot OH \quad (7)$$

$$h^+,\ \cdot OH,\ \text{or}\ H_2O_2 + \text{AO7} \rightarrow \text{Degradation products} \quad (8)$$

From Figure 6, it is found that the photocatalytic activity of the composites is highly related to the content of graphene, which can be explained as follows. With raising the graphene content, the amount of $SrTiO_3$ particles decorated on the surface of graphene is expected to increase, thus providing more photogenerated carriers for the photocatalytic reaction. When the graphene content in the composites reaches 7.5%, the $SrTiO_3$ particles are decorated sufficiently, consequently leading to the achievement of the highest photocatalytic activity. However, with further increasing graphene content above 7.5%, the photocatalytic efficiency begins to exhibit a decreasing trend. The possible reason is that the excessive graphene may shield the light and decrease the photon absorption by the $SrTiO_3$ particles, and moreover, the amount of available surface active sites tends to be reduced due to an increasing coverage of graphene onto the surface of the $SrTiO_3$ particles.

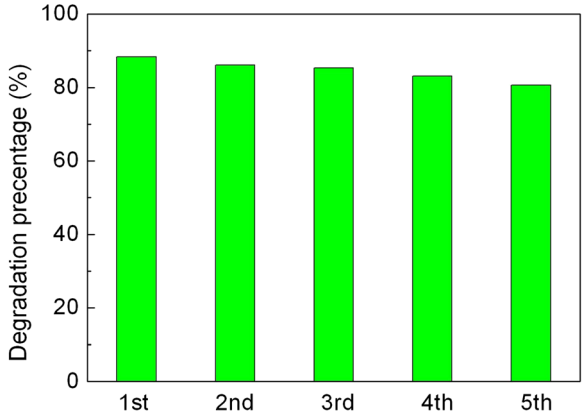

Figure 10 Degradation percentage of AO7 after irradiation for 6 h over $SrTiO_3$-graphene(7.5%) composites during the five photocatalytic cycles.

Besides the photocatalytic activity, the reusability of photocatalysts is another crucial factor for their practical applications. The stability of the $SrTiO_3$-graphene(7.5%) composites is examined by the recycling photocatalytic experiment, as shown in Figure 10. It reveals that the degradation percentage of AO7 maintains 80% to 88% for five consecutive recycles. The tiny or negligible lose of the photocatalytic efficiency indicates the excellent photocatalytic reusability of the as-prepared $SrTiO_3$-graphene composites. Figure 11 shows the XRD patterns of the composites before and after the recycle experiment, revealing no obvious crystal structure changes. Figure 12 shows the TEM images of the composites before and after the recycle experiment, from which one can see that $SrTiO_3$ particles are still well decorated on the graphene sheets.

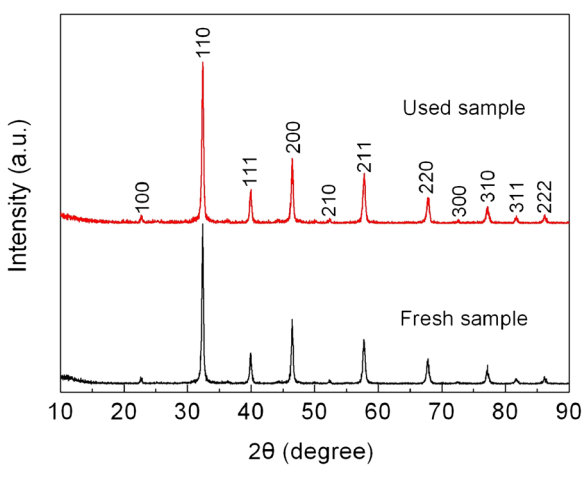

Figure 11 XRD patterns of $SrTiO_3$-graphene(7.5%) composites before and after the photocatalytic experiment.

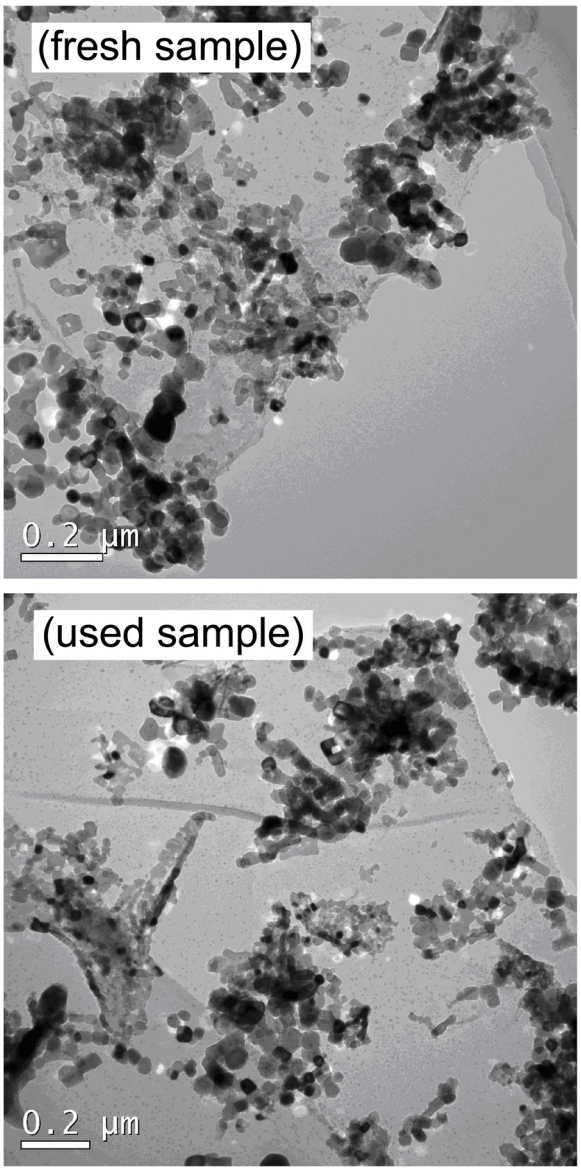

Figure 12 TEM images of the $SrTiO_3$-graphene(7.5%) composites before (top) and after (bottom) the photocatalytic experiment.

Conclusions

$SrTiO_3$-graphene nanocomposites were prepared by irradiating the mixture solution of $SrTiO_3$ nanoparticles and graphene oxide sheets, during which graphene oxide receives electrons from the excited $SrTiO_3$ nanoparticles to be reduced to graphene, simultaneously leading to the assembly of $SrTiO_3$ nanoparticles onto graphene sheets. Compared to the bare $SrTiO_3$ nanoparticles, the as-prepared $SrTiO_3$-graphene composites exhibit an enhanced photocatalytic activity for the degradation of AO7 under irradiation of UV light. This can be attributed to the effective separation of photogenerated electron–hole pairs due to the electron transfer from $SrTiO_3$ to graphene and, hence, increased availability of electrons and holes for the photocatalytic reaction. The enhanced generation of $\cdot OH$ radicals is observed over the irradiated $SrTiO_3$-graphene composites compared to the bare $SrTiO_3$ nanoparticles. The photocatalytic efficiency is slightly deceased by purging with N_2 but is significantly suppressed by the addition of ethanol and KI (especially for the latter). Based on the experimental results, $\cdot OH$, h^+, and H_2O_2 are suggested to be the main active species causing the dye degradation.

Abbreviations

AO: ammonium oxalate; AO7: acid orange 7; CB: conduction band; e^-: photogeneration of electron; E_g: bandgap energy; FTIR: Fourier transform infrared spectroscopy; h^+: photogeneration of hole; H_2O_2: hydrogen peroxide; NHE: normal hydrogen electrode; OH: hydroxyl radicals; PL: photoluminescence; TA: terephthalic acid; TAOH: 2-hydroxyterephthalic acid; TEM: transmission electron microscope; UV: ultraviolet; VB: valence band; XRD: X-ray powder diffraction.

Competing interests

The authors declare that they have no competing interests.

Authors' contributions

HY and TX conceived the idea of experiments. TX, LD, JM, and HZ carried out the preparation and characterization of the samples. HY, TX, and JD analyzed and discussed the results of the experiments. TX drafted the manuscript. HY improved the manuscript. All authors read and approved the final manuscript.

Authors' information

HY is a professor and a Ph.D. degree holder specializing in the investigation of photocatalytic and nanometer materials. JD is a professor and a Ph.D. degree holder specializing in the investigation of nanometer materials. JM and HZ are instructors and M.Sc. degree holders specializing in the research of nanometer materials. TX is a doctoral candidate major in the study of photocatalytic materials. LD is a graduate student major in the preparation of photocatalytic materials.

Acknowledgements

This work was supported by the National Natural Science Foundation of China (Grant No. 51262018) and the Hongliu Outstanding Talents Foundation of Lanzhou University of Technology (Grant No. J201205).

Received: 24 April 2014 Accepted: 20 June 2014
Published: 29 June 2014

References

1. Mills A, Davies RH, Worsley D: **Water purification by semiconductor photocatalysis.** *Chem Soc Rev* 1993, **22:**417–425.
2. Hofmann MR, Martin ST, Choi W, Bahnemann DW: **Environmental applications of semiconductor photocatalysis.** *Chem Rev* 1995, **95:**69–96.
3. Zheng Z, Huang B, Qin X, Zhang X, Dai Y: **Facile synthesis of $SrTiO_3$ hollow microspheres built as assembly of nanocubes and their associated photocatalytic activity.** *J Colloid Interface Sci* 2011, **358:**68–72.
4. Kato H, Kobayashi M, Hara M, Kakihana M: **Fabrication of $SrTiO_3$ exposing characteristic facets using molten salt flux and improvement of photocatalytic activity for water splitting.** *Catal Sci Technol* 2013, **3:**1733–1738.
5. da Silva LF, Avansi W, Andres J, Ribeiro C, Moreira ML, Longo E, Mastelaro VR: **Long-range and short-range structures of cube-like shape $SrTiO_3$ powders: microwave-assisted hydrothermal synthesis and photocatalytic activity.** *Phys Chem Chem Phys* 2013, **15:**12386–12393.
6. Kuang Q, Yang S: **Template synthesis of single-crystal-like porous $SrTiO_3$ nanocube assemblies and their enhanced photocatalytic hydrogen evolution.** *ACS Appl Mat Interfaces* 2013, **5:**3683–3690.
7. Cao T, Li Y, Wang C, Shao C, Liu Y: **A facile in situ hydrothermal method to $SrTiO_3$/TiO_2 nanofiber heterostructures with high photocatalytic activity.** *Langmuir* 2011, **27:**2946–2952.

8. Puangpetch T, Chavadej S, Sreethawong T: **Hydrogen production over Au-loaded mesoporous-assembled $SrTiO_3$ nanocrystal photocatalyst: effects of molecular structure and chemical properties of hole scavengers.** *Energy Convers Manage* 2011, **52:**2256–2261.
9. Guoa J, Ouyang S, Li P, Zhang Y, Kako T, Ye J: **A new heterojunction Ag_3PO_4/Cr-$SrTiO_3$ photocatalyst towards efficient elimination of gaseous organic pollutants under visible light irradiation.** *Appl Catal B Environ* 2013, **134–135:**286–292.
10. Zou F, Jiang Z, Qin X, Zhao Y, Jiang L, Zhi J, Xiao T, Edwards PP: **Template-free synthesis of mesoporous N-doped $SrTiO_3$ perovskite with high visible-light-driven photocatalytic activity.** *Chem Commun* 2012, **48:**8514–8516.
11. Bolotin KI, Sikes KJ, Jiang Z, Klima M, Fudenberg G, Hone J, Kim P, Stormer HL: **Ultrahigh electron mobility in suspended graphene.** *Solid State Commun* 2008, **146:**351–355.
12. Balandin AA, Ghosh S, Bao W, Calizo I, Teweldebrhan D, Miao F, Lau CN: **Superior thermal conductivity of single-layer graphene.** *Nano Lett* 2008, **8:**902–907.
13. Frank IW, Tanenbaum DM, Van Der Zande AM, McEuen PL: **Mechanical properties of suspended graphene sheets.** *J Vac Sci Technol B* 2007, **25:**2558–2561.
14. Xu TG, Zhang LW, Cheng HY, Zhu YF: **Significantly enhanced photocatalytic performance of ZnO via graphene hybridization and the mechanism study.** *Appl Catal B Environ* 2011, **101:**382–387.
15. Cuong TV, Pham VH, Tran QT, Chung JS, Shin EW, Kim JS, Kim EJ: **Optoelectronic properties of graphene thin films prepared by thermal reduction of graphene oxide.** *Mater Lett* 2010, **64:**765–767.
16. Lü W, Chen J, Wu Y, Duan L, Yang Y, Ge X: **Graphene-enhanced visible-light photocatalysis of CdS particles for wastewater treatment.** *Nanoscale Res Lett* 2014, **9:**148.
17. Gao M, Peh CKN, Ong WL, Ho GW: **Green chemistry synthesis of a nanocomposite graphene hydrogel with three-dimensional nanomesopores for photocatalytic H_2 production.** *RSC Advances* 2013, **3:**13169–13177.
18. Liu X, Pan L, Zhao Q, Lv T, Zhu G, Chen T, Lu T, Sun Z, Sun C: **UV-assisted photocatalytic synthesis of ZnO-reduced graphene oxide composites with enhanced photocatalytic activity in reduction of Cr(VI).** *Chem Eng J* 2012, **183:**238–243.
19. Wong TJ, Lim FJ, Gao M, Lee GH, Ho GW: **Photocatalytic H_2 production of composite one-dimensional TiO_2 nanostructures of different morphological structures and crystal phases with graphene.** *Catal Sci Technol* 2013, **3:**1086–1093.
20. Bell NJ, Ng YH, Du A, Coster H, Smith SC, Amal R: **Understanding the enhancement in photoelectrochemical properties of photocatalytically prepared TiO_2-reduced graphene oxide composite.** *J Phys Chem C* 2011, **115:**6004–6009.
21. Akhavan O: **Graphene nanomesh by ZnO nanorod photocatalysts.** *ACS Nano* 2010, **7:**4174–4780.
22. Li Z, Zhou Z, Yun G, Shi K, Lv X, Yang B: **High-performance solid-state supercapacitors based on graphene-ZnO hybrid nanocomposites.** *Nanoscale Res Lett* 2013, **8:**473.
23. Yan Z, Ma L, Zhu Y, Lahiri I, Hahm MG, Liu Z, Yang S, Xiang C, Lu W, Peng Z, Sun Z, Kittrell C, Lou J, Choi W, Ajayan PM, Tour JM: **Three-dimensional metal-graphene-nanotube multifunctional hybrid materials.** *ACS Nano* 2013, **7:**58–64.
24. Liang Y, Li Y, Wang H, Zhou J, Wang J, Regier T, Dai H: **Co_3O_4 nanocrystals on graphene as a synergistic catalyst for oxygen reduction reaction.** *Nat Mater* 2011, **10:**780–786.
25. Xian T, Yang H, Dai JF, Wei ZQ, Ma JY, Feng WJ: **Photocatalytic properties of $SrTiO_3$ nanoparticles prepared by a polyacrylamide gel route.** *Mater Lett* 2011, **21–22:**3254–3257.
26. Kosmulski M: **pH-dependent surface charging and points of zero charge. IV. Update and new approach.** *J Colloid Interface Sci* 2009, **337:**439–448.
27. Talyzin AV, Hausmaninger T, You S, Szabob T: **The structure of graphene oxide membranes in liquid water, ethanol and water-ethanol mixtures.** *Nanoscale* 2014, **6:**272–281.
28. Liu W, Wang M, Xu C, Chen S, Fu X: **Significantly enhanced visible-light photocatalytic activity of g-C_3N_4 via ZnO modification and the mechanism study.** *J Mol Catal A Chem* 2013, **9–15:**368–369.
29. Last JT: **Infrared-absorption studies on barium titanate and related materials.** *Phys Rev* 1957, **105:**1740–1750.
30. Zhao D, Sheng G, Chen C, Wang X: **Enhanced photocatalytic degradation of methylene blue under visible irradiation on graphene@TiO_2 dyade structure.** *Appl Catal B Environ* 2012, **111–112:**303–308.
31. Teoh WY, Scott JA, Amal R: **Progress in heterogeneous photocatalysis: from classical radical chemistry to engineering nanomaterials and solar reactors.** *J Phys Chem Lett* 2012, **3:**629–639.
32. Daneshvar N, Salari D, Khataee AR: **Photocatalytic degradation of azo dye acid red 14 in water: investigation of the effect of operational parameters.** *J Photochem Photobiol A Chem* 2003, **157:**111–116.
33. Li YY, Wang JS, Yao HC, Dang LY, Li Z: **Efficient decomposition of organic compounds and reaction mechanism with BiOI photocatalyst under visible light irradiation.** *J Mol Catal A Chem* 2011, **334:**116–122.
34. Morrison SR: *Electrochemistry at Semiconductor and Oxidized Metal Electrode.* New York: Plenum; 1980.
35. Hotop H, Lineberger WC: **Binding energies in atomic negative ions.** *J Phys Chem Ref Data* 1975, **4:**539–576.
36. Andersen T, Haugen HK, Hotop H: **Binding energies in atomic negative ions: III.** *J Phys Chem Ref Data* 1999, **28:**1511–1533.
37. Zhang J, Yu J, Jaroniec M, Gong JR: **Noble metal-free reduced graphene oxide-$Zn_xCd_{1-x}S$ nanocomposite with enhanced solar photocatalytic H_2-production performance.** *Nano Lett* 2012, **12:**4584–4589.
38. Arai T, Yanagida M, Konishi Y, Iwasaki Y, Sugihara H, Sayama K: **Efficient complete oxidation of acetaldehyde into CO_2 over $CuBi_2O_4/WO_3$ composite photocatalyst under visible and UV light irradiation.** *J Phys Chem C* 2007, **111C:**7574–7577.
39. Tachikawa T, Fujitsuka M, Majima T: **Mechanistic insight into the TiO_2 photocatalytic reactions: design of new photocatalysts.** *J Phys Chem C* 2007, **111C:**5259–5275.

doi:10.1186/1556-276X-9-327
Cite this article as: Xian *et al.*: Photocatalytic reduction synthesis of $SrTiO_3$-graphene nanocomposites and their enhanced photocatalytic activity. *Nanoscale Research Letters* 2014 **9**:327.